IOP Publishing and International Atomic Energy Agency Nuclear Fusion
Nucl. Fusion **52** (2012) 054004 (10pp) doi:10.1088/0029-5515/52/5/054004

First use of three-dimensional equilibrium, stability and transport calculations for interpretation of ELM triggering with magnetic perturbations in NSTX

J.M. Canik[1], S.P. Hirshman[1], R. Sanchez[2], R. Maingi[1], J.-W. Ahn[1], R.E. Bell[1], A. Diallo[1], S.P. Gerhardt[3], B.P. LeBlanc[3], J.E. Menard[3], J.-K. Park[3], M. Podesta[1] and S.A. Sabbagh[4]

[1] Oak Ridge National Laboratory, PO Box 2008, Oak Ridge, TN 37831, USA
[2] Departamento de Fisica, Universidad de Carlos de Madrid, Leganes 28021, Spain
[3] Princeton Plasma Physics Laboratory, PO Box 451, Princeton, NJ 08543, USA
[4] Columbia University, 116th Street and Broadway, New York, NY 10027, USA

Received 18 June 2011, accepted for publication 25 January 2012
Published 9 May 2012
Online at stacks.iop.org/NF/52/054004

Abstract
The application of non-axisymmetric magnetic perturbations has been demonstrated to destabilize edge-localized modes (ELMs) in the National Spherical Torus Experiment. A model 3D equilibrium has been calculated for these experiments using the VMEC code, which assumes nested flux surfaces and therefore that resonant perturbations are shielded. First, a free-boundary equilibrium is calculated using the NSTX coil set, with pressure and current profiles matched to a standard 2D reconstruction, but with up–down symmetry enforced. A new equilibrium is then calculated with the $n = 3$ field applied at a level consistent with experiment. This equilibrium is then used as the basis of further calculations using codes developed for analysis of stellarator plasmas. The neoclassical transport due to the 3D fields is calculated to be small compared with the experimental transport rates. Initial stability analysis has been performed, and indicates a modest degradation in ballooning stability with 3D fields applied. A new 3D equilibrium is also calculated using the SIESTA code, which allows for the formation of islands and stochastic regions. A comparison of the field structure between the SIESTA calculation and the assumption of fully penetrated vacuum perturbation indicates smaller island sizes and very small stochastic transport in the SIESTA case.

(Some figures may appear in colour only in the online journal)

1. Introduction

While nominally axisymmetric, the effects of small 3D magnetic perturbations have proven to have a strong impact on the performance of tokamak plasmas. In particular, the application of resonant magnetic perturbations has been studied intensively recently [1–4], since this may provide a means of controlling edge-localized mode (ELM) size [5] in future large experiments such as ITER. While such 3D fields have been observed experimentally to have a strong impact on transport and stability, these effects are not well understood, introducing significant uncertainty in extrapolating the use of 3D fields as control tools in large future devices.

The impact of 3D magnetic perturbations on plasma behaviour in the National Spherical Torus Experiment [6] is a case where experimental results are not well understood theoretically. As will be shown, the result of applying $n = 3$ fields is the rather robust triggering of ELMs in otherwise ELM-free H-modes [2, 7], with the change in stability only partially explained by the observed pedestal profile changes. The impact of $n = 3$ fields on pedestal transport and profiles is less consistent, with the pressure gradient increasing in some cases [2] and local flattening of the electron temperature and density observed in others [8].

In this paper, we describe the application of stellarator tools to help analyse these NSTX experiments. These codes have been developed over several decades to study the equilibrium, stability and transport properties in systems that are inherently 3D, and so are well suited to analysing the effects of 3D perturbations to tokamaks. The first step

in these studies is the generation of 3D MHD equilibria that include the non-axisymmetric perturbations. Here, two types of equilibria are studied: an ideal 3D equilibrium with closed flux surfaces (using the VMEC code [9]), and a quasi-resistive equilibrium allowing for the possibility of magnetic island formation (using the SIESTA code [10]). To facilitate this work, several approximations are made as described in more detail below. For example, the plasma is assumed to be up–down symmetric, whereas the experiments deviate somewhat from this symmetry (this approximation is required by the transport and stability codes that couple to the VMEC equilibrium, as well as by SIESTA). Another approximation is made regarding the pressure and current profiles used in the 3D modelling. In order to produce a VMEC equilibrium, first a 2D plasma reconstruction generated using conventional tokamak analysis tools must be transferred into an equivalent VMEC calculation. While the highest-fidelity 2D plasma reconstruction available at present was used to make this transfer, the pressure and current profiles do not fully capture the experimental pedestal structure. These approximations prevent us from performing a comprehensive study of the stability of the experimental plasmas. However, the resulting model equilibria do allow the study of how properties change when 3D fields are applied, which is the focus of this paper.

Several codes are available that couple to the ideal equilibrium from VMEC to calculate, e.g., neoclassical transport and MHD stability in 3D fields. Two sets of such calculations are presented here: the neoclassical flux induced by the breaking of axisymmetry, and the stability to infinite-n ballooning modes. As will be shown, the ripple-induced neoclassical transport is negligibly small compared with the experimental cross-field transport rates, so that this transport mechanism should not impact the edge density and temperature profiles. In addition, a preliminary analysis of MHD stability shows that the 3D field application degrades ballooning stability, but as will be argued the magnitude of the stability change is small. In the future, this analysis will be extended to include finite-n stability (more relevant for ELMs), as well as edge pressure and current profiles more consistent with experiment.

Finally, a new equilibrium calculated with the SIESTA code, which allows for island formation, is studied. The SIESTA equilibrium shows that, even though the applied fields have strong resonant components, the islands produced when plasma response is included and MHD equilibrium is enforced are for the most part rather small. As a result, the stochasticity of the magnetic field is small when compared with that calculated using the vacuum perturbation fields without the plasma response, and the related stochastic transport rates are estimated to be small compared with experiment.

This paper is organized as follows. In section 2, a brief review of the observations from ELM destabilization experiments is given, along with simple estimates of the stochastic transport rates calculated when the plasma response is neglected. Section 3 describes the calculation of an ideal, nested-flux-surface 3D equilibrium using the VMEC code. The following two sections present calculations based on this VMEC equilibrium, with neoclassical transport addressed in section 4 and ballooning stability in section 5. The calculation of a new equilibrium with SIESTA, allowing for the presence of islands, is presented in section 6. Section 7 contains a discussion of the results obtained to date, and a description of further research plans.

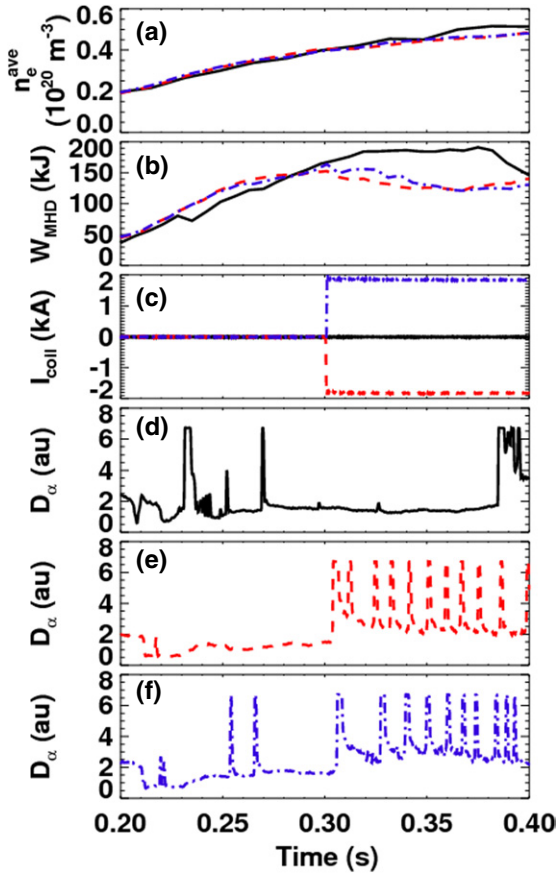

Figure 1. Time traces of (*a*) line-averaged electron density, (*b*) plasma stored energy, (*c*) current in perturbation coils, and (*d*)–(*f*) divertor D_α emission during control discharge (solid black), with $n = 3$ field applied (red/dashed), and with $n = 3$ applied with phase shifted by 60° (blue/dotted–dashed).

2. Overview of ELM-triggering experiments in NSTX

The triggering of ELMs by magnetic perturbations has been robustly observed in NSTX. An example is shown in figure 1, where in the control case without applied 3D fields the plasma shows a long phase free of large ELMs. With an $n = 3$ field applied, ELMs are destabilized, with several ELMs occurring in the presence of the static perturbation. Similar destabilization is also observed when a perturbation of the opposite phase is applied. This destabilization of ELMs during otherwise ELM-free phases is routinely observed in NSTX when sufficiently strong $n = 3$ fields are applied. This includes plasmas where thick layers of lithium are deposited on the PFCs prior to the discharge [11]. These coatings result in a relaxation of the pedestal profile [12], which makes the edge strongly stable to ELMs [13]. Even with the stabilizing effect of lithium, 3D fields destabilize ELMs, and pulsed $n = 3$ fields have been used for ELM pacing to control impurity content during these discharges with lithium coated PFCs [14].

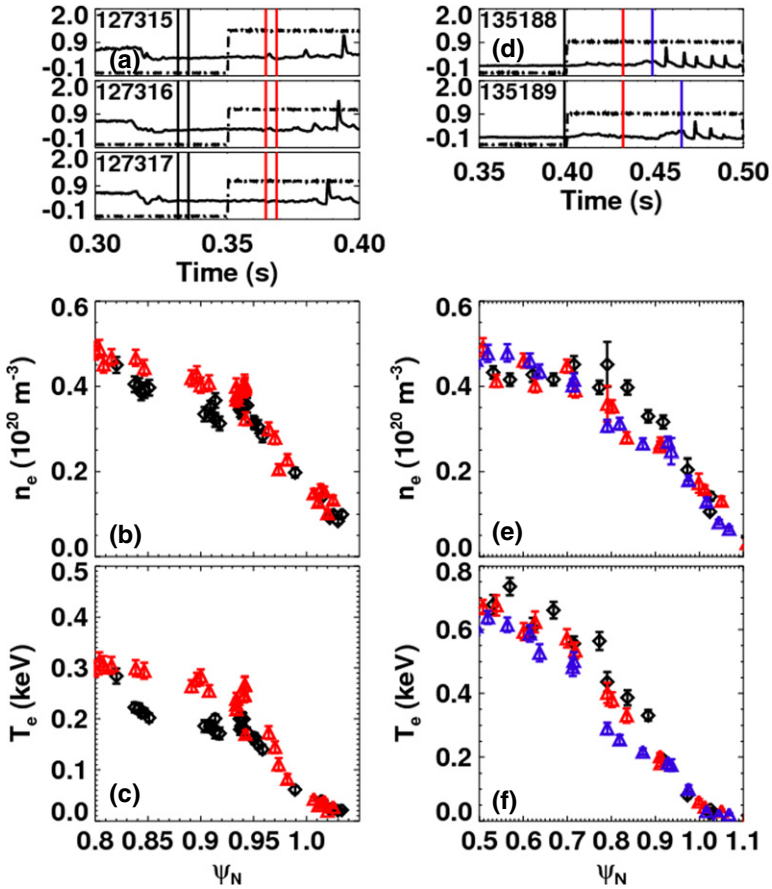

Figure 2. (*a*) Perturbation coil current (dashed) and D_α (solid), with profile measurement times indicated by vertical lines, (*b*) electron density and (*c*) temperature profiles without (black) and with (red) 3D field applied with no lithium coatings. (*d*)–(*f*) same, but with lithium coatings, with an additional time point shown just prior to ELM onset (blue).

The effect of 3D fields on pedestal transport and structure is less consistent than the ELM-triggering effect. Panels (*b*) and (*c*) of figure 2 show pedestal profiles during initial experiments testing the effects of 3D fields that were performed without any lithium coatings [2]. These profiles combine data from several time slices and multiple shots; these time slices are indicated by the vertical lines in panel (*a*) (with colours corresponding to those of the profiles), which also shows the timing of the profile measurements relative to the 3D field application and ELM onset. In this case, the density profile is largely unchanged; 'density pumpout', which has been seen on other experiments during RMP application [15, 16], is generally not observed on NSTX (a second example can be seen in figure 1, where the line-averaged density evolution is unchanged by the applied 3D field). The pedestal electron temperature, on the other hand, *increases* with the 3D field applied. This gives an increase in the pedestal pressure gradient, which was calculated to be sufficient to destabilize peeling–ballooning modes [2]. However, in later experiments, similar profile measurements were repeated in discharges with lithium coated plasma PFCs, and this increase in the edge T_e was not observed. Instead, as shown in panels (*d*)–(*f*) of figure 2, a local flattening is seen in the region from $\psi_N \sim 0.8$–0.9, in both the electron density and temperature. The profiles outside of $\psi_N \sim 0.9$ are not strongly affected by the 3D fields. Even though the pressure gradient is not increased in this case, ELMs are still destabilized, suggesting a more universal cause than the pressure steepening to which the triggering was originally attributed. Thus, the modifications to the pedestal profiles induced by the 3D fields and the changes to ELM stability remain poorly understood. The case without any lithium coatings is the focus of the studies presented in this paper. Note that in all cases a reduction in toroidal rotation is observed across the plasma profile, as expected from neoclassical toroidal viscosity [17, 18].

2.1. Estimates of stochastic transport

For later comparisons with models that include plasma response, estimates have been made of the stochastic transport in the case that this response is neglected. The simple superposition of the 2D equilibrium magnetic field with 3D vacuum fields from the perturbation coils (the so-called 'vacuum paradigm' [19]) predicts a high level of stochasticity [7]. This can be seen by estimating the expected effect of the stochastic transport, which is based on the field line diffusivity calculated as $D_{FL} = \langle(\Delta r)^2\rangle/2L$, where Δr is the radial excursion of a field line in a step of distance L along the field line [20]. D_{FL} is calculated using the vacuum perturbation, and then used in conjunction with the plasma kinetic profiles to estimate the stochastic particle and electron thermal diffusivities D and χ_e. These are then compared with

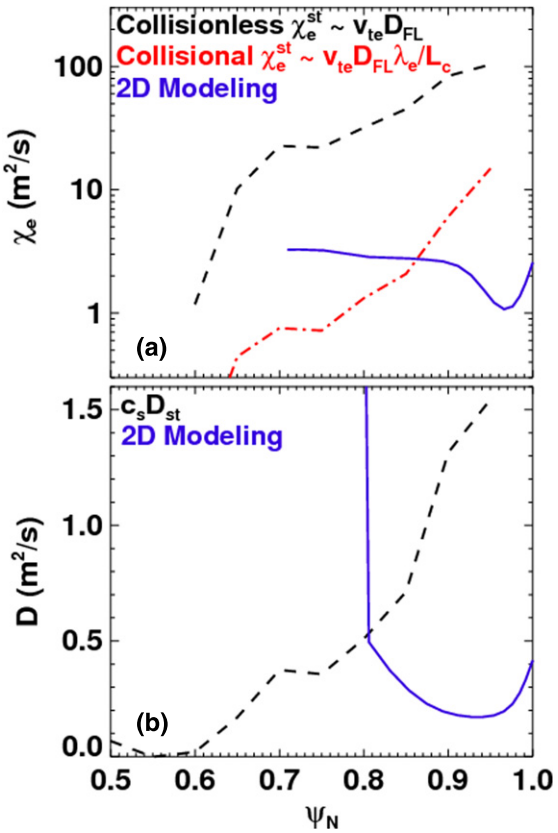

Figure 3. Profiles of (*a*) electron thermal and (*b*) particle diffusivity due to stochastic transport (dashed black/red) and inferred from 2D modelling of experiment (solid blue).

the values inferred from experiment, which are obtained by 2D interpretive modelling of the edge plasma [21] using the SOLPS [22] suite of codes, which allows a self-consistent treatment of the scrape-off layer plasma and recycling neutrals (this method has been successfully benchmarked against several other approaches to determine transport coefficients at the plasma edge [23], although uncertainty in the fraction of power carried by different particle species can have large (∼50%) effects on the inferred heat transport rates).

A simple estimate of the stochastic transport of electron heat in the absence of collisions is made by multiplying the magnetic diffusivity by the electron thermal velocity [24]. This yields a thermal diffusivity that is much larger than the value from SOLPS modelling across the plasma radius, as shown in figure 3. At high collisionality, the stochastic thermal diffusivity can be reduced from this collisionless level [25]. Even with the collisional factor accounted for, however, the stochastic electron thermal diffusivity is large compared with the SOLPS values in the pedestal region, which extends from $\psi_N = 0.92$–1.0. The situation is similar for particle transport. A rigorous derivation of the particle transport requires an accounting of the ambipolar radial electric field, since the electrons will tend to stream radially along open field lines more quickly than ions. This will drive the electric field positive, which will tend to reduce the electron particle flux down to the level of the slower ions. The impact of stochasticity on the radial electric field has been shown experimentally; see, e.g., [26]). A rough estimate of the ambipolar flux can be made by multiplying the field line diffusivity by the plasma sound speed $c_s = \sqrt{(T_e + T_i)/m_i}$. Indeed, a related model has been successful in reproducing the density profile changes measured in RMP experiments at DIII-D [27]. This estimate yields particle transport rates that are larger than the values inferred from edge modelling in the pedestal region (panel (*b*) of figure 3). These admittedly simple estimates of stochastic transport (more rigorous calculations using 3D fluid transport modelling is underway [28]) indicate that, if this field were present in experiment, the 3D fields should have an impact on the edge profiles—especially T_e. However, as shown in figure 2, strong changes are not seen. These observations indicate that the plasma response to the applied perturbations cannot be neglected, and is likely to result in a reduction in the stochasticity of the magnetic field. An analysis of the nonlinear plasma response can be performed, at least approximately, using the 3D equilibrium codes described below.

3. Generation of 3D equilibrium

The first step in analysing the NSTX experiments using stellarator codes is to generate a 3D equilibrium using the VMEC code. VMEC uses a variational approach to minimize the total plasma energy

$$W = \int \left(\frac{|B|^2}{2\mu_0} + \frac{p}{\gamma - 1} \right) \mathrm{d}^3 x,$$

where γ is the adiabatic index, yielding a solution to ideal MHD force balance $F = J \times B - \nabla p = 0$. VMEC is fully three-dimensional with no restrictions on symmetry, and can be used either in fixed or free-boundary mode. The magnetic field is assumed to take a Clebsch form [29]. An inverse coordinate representation [30] is used in which the cylindrical coordinates $R(s, \theta, \phi)$, $Z(s, \theta, \phi)$, are treated as the dependent variables in the variation of W, while the flux coordinates (s, θ, ϕ) are treated as independent variables. Here s is a flux surface label (normalized toroidal flux is used in VMEC), and θ and ϕ are poloidal and toroidal angles, respectively. The method used in VMEC requires nested magnetic flux surfaces, and cannot treat islands or stochastic regions. VMEC therefore solves for the ideal 3D equilibrium, with current sheets at rational surfaces perfectly cancelling any resonant components in the 3D field. In this sense the VMEC equilibrium gives the magnetic field assuming perfect shielding of the perturbation, e.g. by plasma rotation [31] (although VMEC does not include rotation in the force balance equation).

Before generating a 3D equilibrium, the profiles of pressure and safety factor arising from a 2D equilibrium reconstruction are transferred in to VMEC. The 2D Grad–Shafranov solution is calculated using the LRDFIT code[5], which is constrained by several measurements including external magnetics, magnetic pitch angle measured by a motional Stark effect [32] diagnostic and corrected for the radial electric field, and with a T_e isotherm constraint that requires that the temperature measured by Thomson scattering [33] be the same on a flux surface on the inner and outer side of the midplane. This is the most highly constrained reconstruction available, but it is not constrained directly by

[5] http://w3.pppl.gov/∼jmenard/software/lrd?t/lrd?t-index.htm

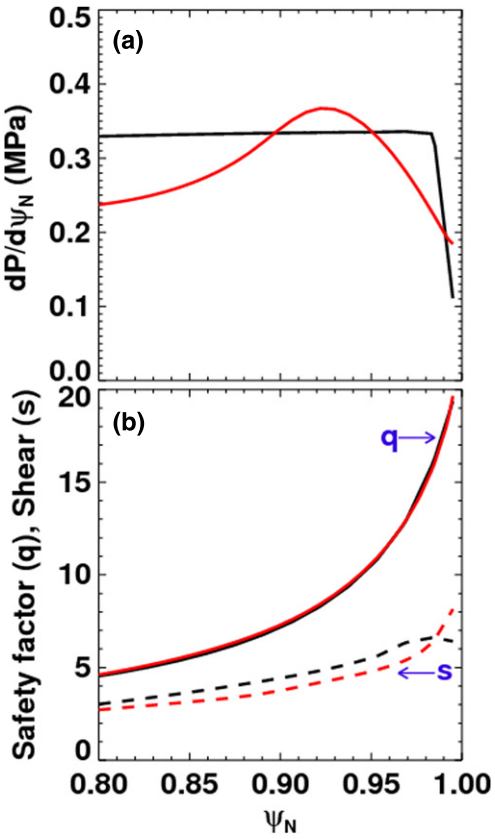

Figure 4. Edge profiles of (*a*) pressure gradient and (*b*) safety factor and shear from the 2D reconstruction usde here (black) and the measured pressure profile and inferred bootstrap current included (red).

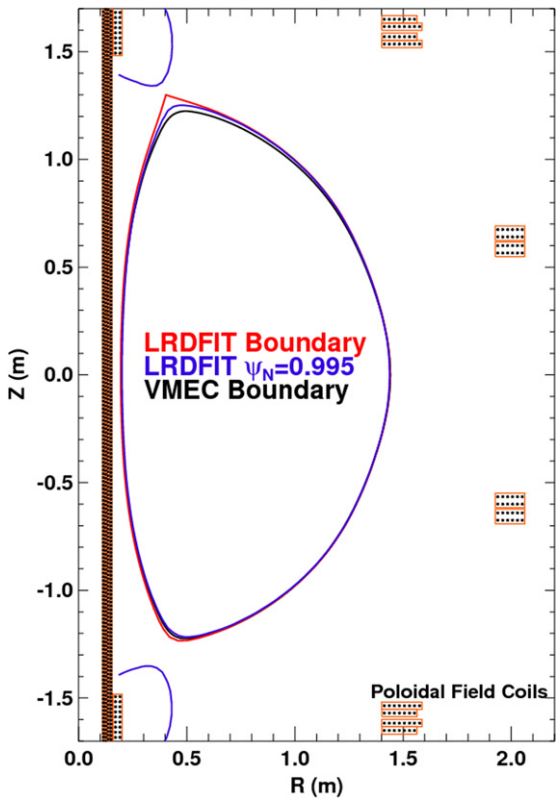

Figure 5. Plasma boundaries from LRDFIT and VMEC codes, and poloidal coil set used in the free-boundary calculations.

the measured kinetic plasma profiles, and the edge current is not constrained to be consistent with the calculated bootstrap current; these are generally needed to accurately calculate the peeling–ballooning stability [34]. While fixed-boundary equilibria are available for these discharges that include these edge constraints (but fewer overall constraints), at present these cannot be transferred into VMEC due to a lack of fast ion pressure (which contributes substantially to the total β in NSTX [35]), without which the position of the plasma cannot be reproduced. A comparison of the edge pressure gradient, safety factor q, and magnetic shear $s = (r/q)(\mathrm{d}q/\mathrm{d}r)$ from the 2D reconstruction used as the basis of the analysis here (black curves), and the same values using the measured pressure profile and inferred bootstrap current (red curves) is shown in figure 4. The reconstruction used here overestimates the pressure gradient over most of the plasma edge, except near the pedestal top at $\psi_N \sim 0.93$, where the experimental gradient is ~10% larger. The safety factor used in these studies is very similar to that obtained when the edge bootstrap current is included, and the reconstructed magnetic shear is ~10–15% larger than with the bootstrap current.

Since the goal of this work is to study the *change* in plasma properties when 3D fields are applied (especially large changes, rather than subtle effects) and not to explain the behaviour of any single case, this reconstruction is considered sufficiently close to the measured edge profiles to serve as a useful starting point for the studies presented here. Further, the robustness of the results to the edge profiles has been checked by generating a new set of VMEC equilibria in which the edge pressure and safety factor have been altered to better match the measurements (the plasma position in this case departs from experiment, with the boundary being shifted on the order of centimetres). Using the altered profiles yields qualitatively similar results for the subsequent transport and stability calculations, and does not change the conclusions drawn. Therefore, in all calculations presented here, the profiles from the 2D reconstruction shown in black in figure 4 are used. When available, higher fidelity reconstructions including the edge kinetic profiles and bootstrap current will be used to improve on this aspect as part of future research, which will allow a more comprehensive study—in particular of the plasma stability—than is presented here.

To compare the VMEC and LRDFIT equilibria, VMEC is first run in a 2D mode with no non-axisymmetric perturbations applied. The pressure and safety factor profiles are read from the LRDFIT output and used as input to VMEC, but are truncated at $\psi_N = 0.995$ to avoid the X-point. VMEC is then run in free-boundary mode, using the experimental coil currents and positions. Although it is not required for VMEC, the code is run in a mode where 'stellarator symmetry' is enforced (in the 2D case, this requires up–down symmetry); this is often required in other codes that use the VMEC equilibrium, and so is enforced here so that these codes can be used to calculate, e.g., the neoclassical transport and stability properties of the equilibrium as described below. This is not viewed as a strong limitation, as the deviation from up–down symmetry is small (see figure 5), and the triggering of ELMs

by 3D fields is robust to small shape changes such as this. The calculated boundary shapes are shown in figure 5, and show that the VMEC calculation reproduces the LRDFIT boundary to within the constraint of up–down symmetry (note that the VMEC boundary is equivalent to the $\psi_N = 0.995$ contour from LRDFIT, due to the truncation of the equilibrium).

Next, a new VMEC equilibrium is calculated which includes the 3D non-axisymmetric magnetic field produced by the perturbation coil set. The perturbation coils are added in the free-boundary VMEC, using a coil current consistent with experiment. VMEC is then rerun using the same profiles of pressure and safety factor as in the 2D case, yielding a new equilibrium that includes the contribution of the 3D fields. The use of the same pressure and safety factor profiles is not justified by experiment, but allows the effect of the 3D fields, which is the emphasis of this paper, to be isolated from profile changes (which are inconsistent, as described in section 2). This process yields two VMEC cases for use in further analysis: one with 3D fields, one without them; these will both be analysed to study the effect of the 3D field on the predicted plasma properties.

4. Neoclassical transport due to 3D fields

The VMEC equilibrium including the 3D perturbation has been used as the basis of neoclassical transport calculations. The breaking of axisymmetry leads to an increase in neoclassical transport at low collisionality [36]. This can be calculated accurately using codes developed for stellarators, where accurate values for the 3D neoclassical transport are needed for the interpretation and design of experiments. To calculate the neoclassical transport, the Boozer magnetic spectrum [37] is calculated. The largest $n \neq 0$ spectral terms are shown in figure 6 for the NSTX 3D field applied case, and are on the order of several 10^{-4} of the total magnetic field. The radial profiles of the spectral components are strongly affected by the shielding currents, which arise at rational surfaces and force the normal component of resonant perturbations to be zero on these surfaces (in the ideal MHD model). This results in non-monotonic radial profiles of the resonant perturbations [38], and similarly affects the radial structure of the Boozer spectrum as shown in figure 6(*a*).

The neoclassical transport induced by the 3D fields can be calculated quickly for the $1/\nu$ regime using the NEO code [39]. This uses a field line tracing technique to give a semi-analytic value of the 'effective ripple' [40] $\varepsilon_{\rm eff}$, which can be used to calculate the transport in the $1/\nu$ regime, where the fluxes scale as $\varepsilon_{\rm eff}^{3/2}$. The radial profile of $\varepsilon_{\rm eff}$ as calculated by NEO is shown in figure 6(*b*), and the corresponding diffusion coefficient as a function of collisionality on a single surface is shown in panel (*c*). For reference, the effective ripple in a conventional stellarator is often on the order of 10% [40], and in optimized stellarators is typically ~1% [41, 42]. Compared with these, the ripple in the NSTX 3D case is rather small, being <0.5% at the plasma edge.

As an initial estimate of the neoclassical fluxes due to the perturbed field, the effective ripple is used to calculate the $1/\nu$ radial particle and heat fluxes. In principle, the radial electric field E_r must be accounted for to accurately calculate neoclassical transport, since transport rates depend sensitively

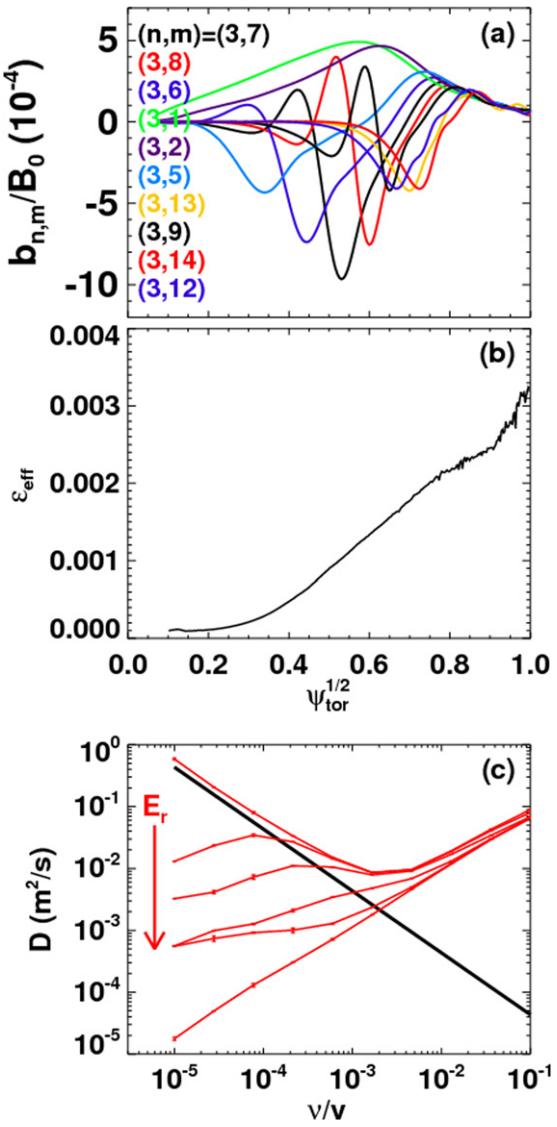

Figure 6. Profile of (*a*) 10 largest non-axisymmetric spectral terms and (*b*) effective ripple; (*c*) NEO (solid black) and DKES (red points) calculated diffusion coefficients (DKES E_r values are $E_r/v = 0, 10^{-5}, 3\times10^{-5}, 10^{-4}, 3\times10^{-4}$ and 10^{-3}).

on E_r, which can change the collisionality dependence and strongly decrease transport. This is typically done by calculating the 'ambipolar' E_r, which yields zero radial charge flux [43]. However, the $1/\nu$ transport regime (neglecting the effect of E_r) is useful to consider on its own, since this gives the largest neoclassical transport rates. As a further approximation, only the electron transport is considered. The motivation for this is that the effect of E_r is stronger for ions, and will generally act to reduce the ion particle flux to the electron level in order to maintain ambipolarity [44] (exceptions to this case exist [45]; however, these 'electron root' scenarios are typically only observed when $\varepsilon_{\rm eff}$ is large or when $T_e \gg T_i$, neither of which is true for NSTX plasmas). Hence, electrons control the total particle transport rate, and by calculating the maximum electron flux one gets a useful measure of how large the total ripple particle flux can be.

The resulting radial electron energy and particle fluxes are shown in figure 7, along with the fluxes from the SOLPS

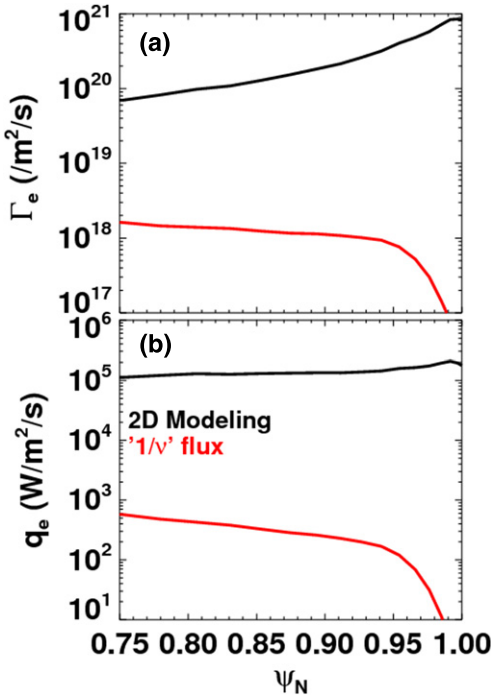

Figure 7. Neoclassical and SOLPS profiles of (*a*) particle and (*b*) electron heat fluxes.

modelling of these experiments. The neoclassical particle and energy fluxes are both much less than the SOLPS values, by nearly two orders of magnitude. Inclusion of the effects of E_r will further reduce Γ^{neo}. Thus, it does not appear that neoclassical transport due to the 3D field is sufficient to measurably increase transport in the pedestal; this is consistent with the lack of transport increase that is measured in experiment. It should be noted that ion neoclassical effects, while not considered here, are likely to be important. These have been studied previously, and for example have been shown to be important for understanding plasma rotation [17, 18].

Although the 3D neoclassical flux is apparently negligible in present NSTX experiments, the collisionality in these experiments is quite high (normalized collisionality $\nu^* \sim 2$ in the case being discussed [2]), which suppresses the $1/\nu$ flux. In contrast, strong density pumpout has been observed in DIII-D experiments at the much lower, more ITER-relevant collisionality of $\nu^* \sim 0.1$ [1]. Further, density pumpout in DIII-D experiments has been observed to become more pronounced at low collisionality [15]. It may be the case that in the neoclassical fluxes are more important in these low-collisionality experiments than in the NSTX discharge analysed here. The neoclassical fluxes may also become large enough to be experimentally relevant in the NSTX Upgrade, which has a goal of operating at reduced collisionality [46]. Since the transport coefficients in the $1/\nu$ regime scale as $D \sim T^{7/2}/n$ [47], if experiments in the NSTX Upgrade were able to achieve three times higher pedestal temperature and half the density (bringing n, T and $\nu*$ in line with those of the DIII-D experiments discussed in [1]), the 3D neoclassical transport would be increased by two orders of magnitude compared with the levels shown in figure 7. Whether these plasma conditions can be attained remains to be seen.

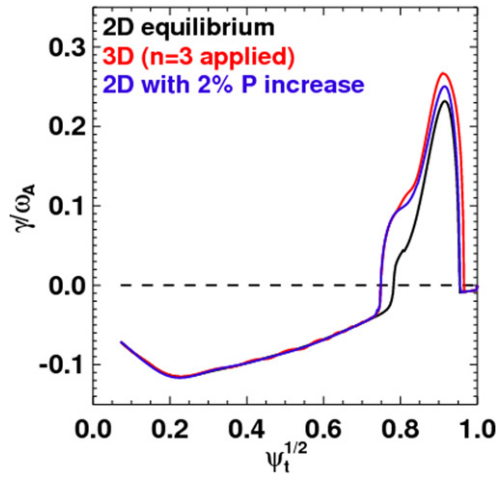

Figure 8. Ballooning growth rates calculated for 2D equilibrium (black), 3D (red) and 2D with pressure increased by 2% (blue).

In such a case where 3D neoclassical transport is likely to be important, a more accurate calculation including the effect of E_r would be necessary. This can be accomplished using the DKES code [48], which calculates the full neoclassical transport matrix for arbitrary magnetic spectrum. This code can be used to build a database of transport coefficients over a range of radial flux surface, collisionality, and radial electric field (an example is shown for a single flux surface in figure 6(*c*)). A further necessity for the tokamak case is to make corrections for momentum conservation. DKES (along with stellarator transport codes in general) do not use momentum conserving collision operators, and as a result do not recover the intrinsic ambipolarity of the neoclassical fluxes in an axisymmetric system. Recently, codes have been developed that correct for this [49, 50], which is likely to be important for correctly calculating the neoclassical ambipolar electric field in a perturbed tokamak.

5. Ballooning stability without and with 3D fields

Since the application of 3D fields to NSTX H-mode plasmas destabilizes ELMs, a long-term goal of this research is to study how the MHD stability properties of the 3D equilibrium differ from those of the 2D case. As discussed above, the edge profiles used in this work differ somewhat from the experimental values (see figure 4), and so at present this can only be accomplished in a preliminary sense. Even so, stability calculations based on these profiles can still be useful for estimating the magnitude of the *change* in stability properties due to 3D fields, even if the stability of the experimental profiles cannot be directly addressed. To this end, an initial study has been performed using the COBRA code [51, 52], which calculates the stability of the VMEC-calculated equilibrium against ballooning modes [53]. Note that in principle, changes to the local curvature and shear of the magnetic field in the presence of stochasticity could affect ballooning stability. However, at present COBRA can only treat the nested-surface magnetic fields as calculated by VMEC, and so cannot analyse these effects in a stochastic field. The results of the COBRA calculation are shown in figure 8, which shows the growth rate for both the 2D case and the case with 3D fields applied.

COBRA calculates a local growth rate [54]; the maximum is shown in figure 8. The position of maximum growth rate is at the outer midplane for both the axisymmetric and non-axisymmetric cases, while the non-axisymmetric case shows in addition a toroidal dependence that follows the $n = 3$ periodicity of the applied field.

The calculation using the 2D equilibrium shows a region near the plasma edge with positive growth rates, indicating instability. This is seemingly at odds with the fact that the plasma is ELM-free in experiment, and does not appear to be simply due to the mismatch of the edge profiles used here with those measured (calculations based on equilibria with the edge profiles altered by hand to better match experiment also show this region of instability with similar growth rates, although the width of the unstable region is reduced by a factor of ∼2). However, this disagreement between experiment and calculation is likely in part due to only infinite-n stability being considered. Peeling–ballooning modes, which are believed to be responsible for ELMs, are most unstable at intermediate n [34], and so finite-n stability must be considered in order to precisely calculate the stability boundary. Indeed, recent analysis of MAST experiments has shown that the pedestal is calculated to be unstable to infinite-n ballooning modes during the period between ELMs, even though the pedestal is experimentally stable [55]. This disagreement is resolved by finite-n calculations, which show stable conditions until just prior to ELM onset. When improved reconstructions with experimentally matched edge profiles become available for the NSTX experiments, studies of finite-n stability will be undertaken. This can be accomplished using other codes developed for stellarators (e.g. the ideal MHD stability code TERPSICHORE [56, 57]), which are capable of assessing low-n stability based on VMEC equilibria.

In the meantime, the change in infinite-n ballooning stability caused by 3D fields can be studied by performing similar COBRA calculations for the equilibrium including the 3D perturbation. As figure 8 shows, with the 3D fields applied the region of instability is enhanced, with both the growth rate within and the radial extent of the unstable region increasing (this change in growth rates is also observed with the altered edge profiles described above). To gauge the magnitude of the change in stability caused by the 3D fields, a second axisymmetric equilibrium has been studied, with the pressure increased by 2%. The ballooning growth rate profile for this case is also shown in figure 8, and is similar to the growth rates for the 3D case (without any pressure scaling). Similarly, reducing the pressure by 2% with 3D fields applied results in similar growth rates (not shown) to the axisymmetric case. This indicates that the stability degradation induced by the 3D field is relatively weak, and would be easily overwhelmed by small changes to the pressure profile. This is consistent with the expectation that non-axisymmetric shaping sufficient to strongly alter stability properties requires significantly larger perturbations than the $\delta B/B \sim 10^{-3}$ applied here [58]. Further, we note that ELM destabilization is also observed during lithiumized ELM-free H-modes [2]. While calculations have not yet been performed for the lithiumized discharges shown in figure 2, the peeling–ballooning stability of other lithiumized discharges has been studied using the ELITE code [34], showing that the plasma is far from the peeling–ballooning stability boundary (see the calculated stability diagram shown in [13], [59]]). In this case, one would expect that small changes to stability such as those calculated here would likely not be sufficient to reach the stability boundary. To test this intuition and explore this regime directly, calculations for experiments starting from lithiumized ELM-free H-mode plasmas, including finite-n stability, will be the focus of future research.

6. Calculation of equilibria with islands with the SIESTA code

A new finite-pressure 3D equilibrium without the restriction of nested flux surfaces has been calculated using the SIESTA code. The SIESTA calculation is based on the VMEC equilibrium, which provides the background coordinate system as well as an initial guess for the equilibrium. Like VMEC, SIESTA also seeks to minimize the total MHD energy. However, SIESTA does not require the magnetic field to be represented in a Clebsch form or use the inverse representation, but instead solves directly for the pressure and magnetic field perturbations in a general form consistent with particle conservation and Faraday's law. This technique allows the code to treat arbitrary magnetic fields without requiring nested flux surfaces, making SIESTA capable of calculating an MHD equilibrium that includes islands and stochastic regions.

SIESTA interleaves ideal and resistive iterations in its solution procedure. During the resistive steps, an artificially large resistivity is added to dissipate the current sheets present at rational surfaces that prevent island formation. In this sense, the SIESTA solution models the magnetic fields assuming full penetration of the magnetic perturbation, as it seeks to fully dissipate the shielding currents. However, unlike the vacuum paradigm, SIESTA includes the nonlinear plasma response (due to finite pressure) and enforces that the final magnetic field satisfy nonlinear MHD force balance. At present, SIESTA is limited to fixed-boundary solutions (with the boundary given by the VMEC 3D equilibrium), and requires stellarator symmetry. These are not fundamental limitations, however, and will be addressed in future versions of the code.

A Poincaré plot using the SIESTA-calculated magnetic field is shown in figure 9, along with a similar plot using the vacuum paradigm for the magnetic perturbation. The SIESTA equilibrium shows magnetic islands at the same radial locations as the vacuum perturbation, as expected since both calculations have the same safety factor profile. However, the islands in the SIESTA case are often significantly smaller, especially towards the plasma edge. The SIESTA solution shows much less island overlap at the plasma edge compared with the vacuum paradigm, and as a result the calculated field line diffusivity using the SIESTA magnetic field is much lower. The resulting stochastic transport rates using the SIESTA fields are similarly reduced, to a level below the values inferred from edge modelling (figure 10). This suggests that the plasma response, even without invoking rotational shielding, prevents edge stochasticity and may explain the lack of increase in electron heat transport. However, it should be noted that these edge islands are likely to be strongly influenced by the boundary conditions used; free-boundary SIESTA calculations will be necessary to explore this effect

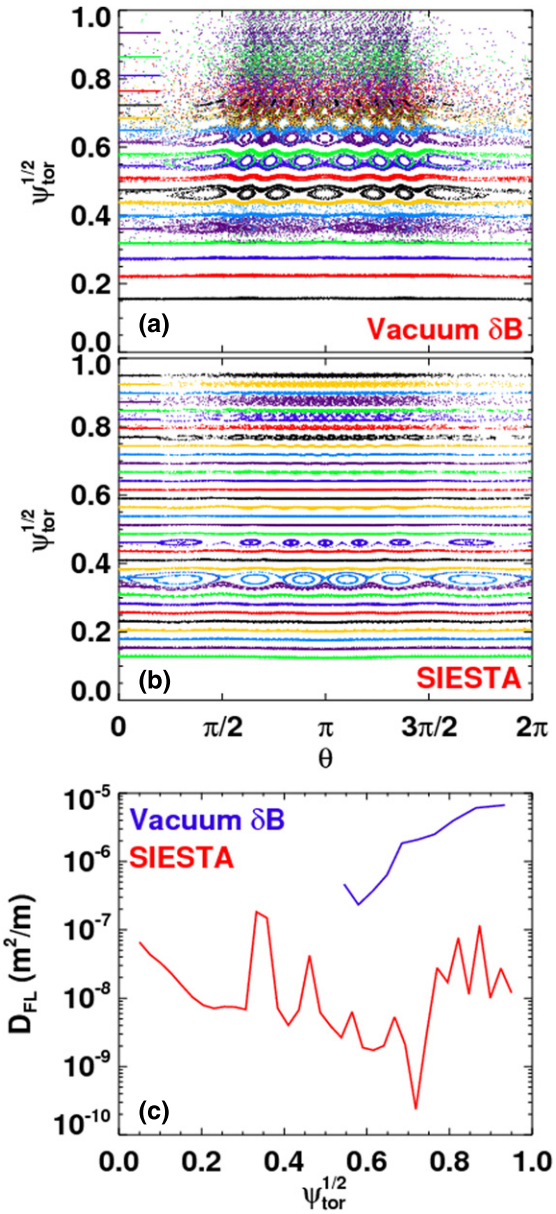

Figure 9. Poincaré plots using the (*a*) vacuum perturbation superposed on 2D equilibrium and (*b*) SIESTA magnetic fields and (*c*) magnetic field line diffusivity using vacuum perturbation (blue) and SIESTA (red) fields.

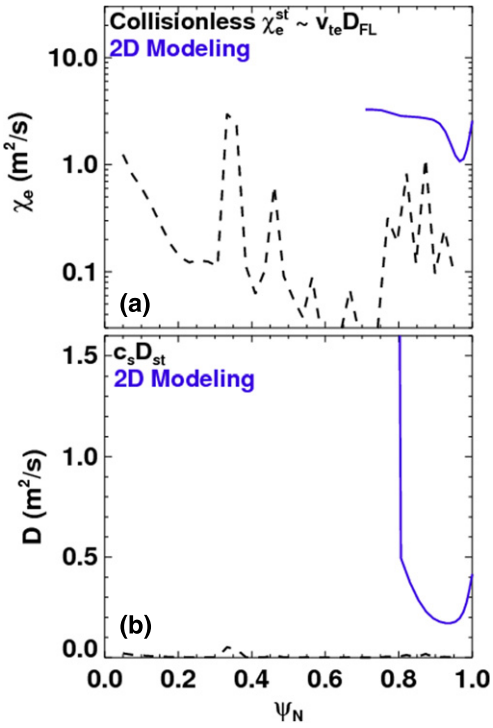

Figure 10. Profiles of (*a*) electron thermal and (*b*) particle diffusivity due to stochastic transport using SIESTA magnetic field (dashed black) and inferred from 2D modelling of experiment (solid blue).

further. In addition, the SIESTA field shows large core islands that experimentally do not appear to be present (based on temperature profiles), indicating that rotational screening of those core islands remains a strong effect.

7. Discussion

An initial analysis of ELM destabilization experiments using 3D fields in NSTX has been performed using tools developed for stellarators. The basis of these calculations is a pair of free-boundary VMEC equilibria: a 2D case, where the plasma boundary from a 2D reconstruction has been reproduced, and a 3D case that includes the magnetic fields from the perturbation coils. While the underlying cause of the ELM triggering has so far not been revealed, several properties of the 3D equilibrium have been studied, with quantification of some of the 3D field effects.

These studies offer some clues to why the experimental edge profiles are not strongly affected by the 3D fields. First, neoclassical transport induced by the non-axisymmetric magnetic field appears to be negligible in present experiments, so that this transport mechanism is too weak to affect the profiles. Further, a SIESTA equilibrium calculation shows that the edge islands are small in the 3D case, with essentially no stochastic transport expected. However, these calculations are fixed-boundary (so that the effects of the 3D coils are not entirely self-consistent and are only described by the 3D VMEC boundary), and do not include rotational screening effects on the perturbations. The importance of screening is evident, for example, in the core islands in the SIESTA calculations whose presence is not supported by experiment. Nonetheless, these calculations are useful for giving an estimate of the maximum stochasticity that can be expected if the perturbations are not screened but fully penetrate the plasma, and it is found that the plasma response has a strong attenuating effect on the perturbations apart from screening.

The plasma stability, which experimentally is consistently and strongly modified by 3D fields, has not been fully addressed here, with a comprehensive analysis being left to future research. However, an initial study has shown that infinite-*n* ballooning stability is modestly degraded by the application of 3D fields, but that the magnitude of this effect is small and can be dominated by small changes to the pressure profile. This suggests that the modification of the stability boundary by 3D fields is too small to explain the observed

triggering, but further calculations are required to test the changes at finite-n.

Several extensions of this work are planned for future research. As described above, a primary focus will be an extension of the stability studies. Calculation will be made of the stability properties of the 3D VMEC equilibrium at low to intermediate n, to study the more relevant peeling–ballooning stability in addition to the pure ballooning stability presented here. Higher fidelity kinetically constrained 2D equilibria, when available, will serve as the starting point for these calculations, so that the edge pressure gradient and current profiles are in better agreement with experiment. In addition, more discharges in which ELM destabilization has been observed will be analysed. This process will allow more accurate, experimentally relevant calculations of the stability of these plasmas, and a more conclusive determination of the effects of 3D fields to be made.

The SIESTA calculations will also be extended to additional discharges, in part to test whether the reduction in island size by the nonlinear plasma response is a possible contributor to the lack of profile response observed, and whether the calculated islands can also explain experiments where local flattening is observed. In order to be conclusive, these results will need to be augmented by calculations using 3D MHD codes that include rotational effects [60, 61]. Finally, further development of the codes used in this study is anticipated, and will allow further physics investigations as new capabilities become available. For example, a free-boundary version of SIESTA would allow a more self-consistent calculation of the effects of the perturbation. Another possible new avenue is exploration of how stochasticity directly affects the MHD stability properties, as opposed to changes due to magnetic flux surface shaping and profile modification. This is outside the capabilities of present codes, but could possibly be accomplished by, e.g., coupling COBRA to the SIESTA equilibrium.

Acknowledgments

This research was supported by the US Department of Energy, Contracts DE-AC05-00OR22725, DE-AC02-09CH11466 and DE-FG02-99ER54524.

References

[1] Evans T.E. *et al* 2008 *Nucl. Fusion* **48** 024002
[2] Canik J.M. *et al* 2010 *Phys. Rev. Lett.* **104** 045001
[3] Kirk A. *et al* 2010 *Nucl. Fusion* **50** 034008
[4] Liang Y. *et al* 2007 *Phys. Rev. Lett.* **98** 265004
[5] Evans T.E. *et al* 2004 *Phys. Rev. Lett.* **92** 235003
[6] Ono M. *et al* 2000 *Nucl. Fusion* **40** 557
[7] Canik J.M. *et al* 2010 *Nucl. Fusion* **50** 034012
[8] Ahn J.-W. *et al* 2010 *Nucl. Fusion* **50** 045010
[9] Hirshman S.P. *et al* 1986 *Comput. Phys. Commun.* **43** 143
[10] Hirshman S.P., Sanchez R. and Cook C.R. 2011 *Phys. Plasmas* **18** 062504
[11] Bell M.G. *et al* 2009 *Plasma Phys. Control. Fusion* **51** 124054
[12] Canik J.M. *et al* 2011 *Phys. Plasmas* **18** 056118
[13] Maingi R. *et al* 2009 *Phys. Rev. Lett.* **103** 075001
[14] Canik J.M. *et al* 2010 *Nucl. Fusion* **50** 064016
[15] Unterberg E.A. *et al* 2009 *J. Nucl. Mater.* **390–391** 486
[16] Alfier A. *et al* 2008 *Nucl. Fusion* **48** 115006
[17] Park J.-K. *et al* 2009 *Phys. Plasmas* **16** 056115
[18] Zhu W. *et al* 2006 *Phys. Rev. Lett.* **96** 225002
[19] Schmitz O. *et al* 2008 *Plasma Phys. Control. Fusion* **50** 124029
[20] Yan L. *et al* 2006 *Nucl. Fusion* **46** 858
[21] Canik J.M. *et al* 2011 *J. Nucl. Mater.* **415** S409
[22] Schneider R. *et al* 2006 *Contrib. Plasma Phys.* **46** 3
[23] Callen J.D. *et al* 2010 *Nucl. Fusion* **50** 064004
[24] Rechester A.B. and Rosenbluth M.N. 1978 *Phys. Rev. Lett.* **40** 38
[25] Joseph I. *et al* 2008 *Nucl. Fusion* **48** 045009
[26] Coenen J.W. *et al* 2011 *Nucl. Fusion* **51** 063030
[27] Mordijck S. *et al* 2010 *Nucl. Fusion* **50** 034006
[28] Lore J.D., Canik J.M., Feng Y., Feng J.-W., Maingi R. and Soukhanovskii V. 2012 *Nucl. Fusion* **52** 054012
[29] D'haeseleer W.D., Hitchon W.N.G., Callen J.D. and Shohet J.L. 1991 *Flux Coordinates and Magnetic Field Structure* (Berlin: Springer)
[30] Hirshman S.P. *et al* 1983 *Phys. Fluids* **26** 3553
[31] Waelbroeck F.L. 2003 *Phys. Plasmas* **10** 4040
[32] Levinton F. and Yuh H. 2008 *Rev. Sci. Instrum.* **79** 10F522
[33] LeBlanc B.P. *et al* 2003 *Rev. Sci. Instrum.* **74** 1659
[34] Snyder P.B. *et al* 2002 *Phys. Plasmas* **9** 2037
[35] Fredrickson E.D. *et al* 2006 *Phys. Plasmas* **13** 056109
[36] Galeev A.A. and Sagdeev R.D. 1977 *Reviews of Plasma Physics* vol 7, ed M.A. Lentovich (New York: Consultants Bureau) p 307
[37] Boozer A.H. 1982 *Phys. Fluids* **25** 520
[38] Park J.-K. *et al* 2007 *Phys. Plasmas* **14** 052110
[39] Nemov V.V. *et al* 1999 *Phys. Plasmas* **6** 4622
[40] Beidler C.D. and Hitchon W.N.G. 1994 *Plasma Phys. Control. Fusion* **36** 317
[41] Canik J.M. *et al* 2007 *Phys. Plasmas* **14** 056107
[42] Reiman A. *et al* 2005 *Nucl. Fusion* **45** 360
[43] Mynick H.E. and Hitchon W.N.G. 1983 *Nucl. Fusion* **23** 1053
[44] Hastings D.E. *et al* 1985 *Nucl. Fusion* **25** 445
[45] Maassberg H. *et al* 2000 *Phys. Plasmas* **7** 295
[46] Menard J.E. *et al* 2010 *Proc. 37th EPS Conf. on Plasma Physics (Dublin, Ireland, 21–25 July 2010)* P.2-106 http://ocs.ciemat.es/EPS2010PAP/pdf/P2.106.pdf
[47] Maassberg H., Beidler C.D. and Simmet E.E. 1999 *Plasma Phys. Control. Fusion* **41** 1135
[48] van Rij W. and Hirshman S.P. 1989 *Phys. Fluids* B **1** 563
[49] Sugama H. and Nishimura S. 2002 *Phys. Plasmas* **9** 4637
[50] Spong D.A. 2005 *Phys. Plasmas* **12** 056114
[51] Sanchez R. *et al* 2000 *J. Comput. Phys.* **161** 576
[52] Sanchez R. *et al* 2001 *Comput. Phys. Commun.* **135** 82
[53] Connor J.W., Hastie R.J. and Taylor R.B. 1979 *Proc. R. Soc. Lond.* A **1** 365
[54] Cuthbert P. and Dewar R.L. 2000 *Phys. Plasmas* **7** 2302
[55] Dickinson D. *et al* 2011 *Plasma Phys. Control. Fusion* **53** 115010
[56] Anderson D.V. *et al* 1990 *J. Supercomput. Appl.* **4** 34
[57] Cooper W.A., Singleton D.B. and Dewar R.L. 1996 *Phys. Plasmas* **3** 275
[58] Boozer A.H. 2009 *Phys. Plasmas* **16** 058102
[59] Boyle D.P. *et al* 2011 *Plasma Phys. Control. Fusion* **53** 105011
[60] Jardin S.C. *et al* 2008 *J. Phys: Conf. Ser.* **125** 012044
[61] Sugiyama L.E. and Park W. 2000 *Phys. Plasmas* **7** 4644